# Feasibility Analysis of Optimal THz bands for passive limb sounding of middle and upper atmospheric wind

Wenyu Wang[1,2], Jian Xu[1], and Zhenzhan Wang[1,2]

[1]National Space Science Center, Chinese Academy of Sciences, Beijing 100190, China
[2]Key Laboratory of Microwave Remote Sensing, National Space Science Center, Chinese Academy of Sciences, Beijing 100190, China

**Correspondence:** Jian Xu (xujian@nssc.ac.cn)

**Abstract.** As of now, direct measurements of middle and upper atmospheric wind are still scarce, and the observation method is limited, especially for the upper stratosphere and lower mesosphere. A new method to derive line-of-sight wind from 30 to more than 120 km is proposed using a high-resolution Terahertz (THz) radiometer, which can fill the measurement gap between lidar and interferometer. Simulations from 0.1 THz to 5 THz for evaluating the feasibility of the spaceborne THz limb
5   sounder are performed in this study. The results show that high-precision wind (better than $5\,\mathrm{m\,s^{-1}}$) can be obtained from 40 to 70 km by covering a cluster of strong $O_3$ lines. By choosing strong $O_2$ or $H_2O$ lines, the high-quality measurement can be extended to 105 km. The O atom (OI) lines can provide wind signals in the higher atmosphere. In addition, performance of different instrument parameters include resolution, bandwidth and measurement noise are analyzed and four different band combinations are suggested at last.

10   **1   Introduction**

Wind is an important meteorological parameter for describing atmospheric dynamical processes. Several studies have already demonstrated that dynamic events occurring in the middle atmosphere have an impact on the tropospheric dynamics and consequently on weather change and climate anomalies in the troposphere (Baldwin and Dunkerton, 2001; Baldwin et al., 2003; Hardiman et al., 2011). The coupling between the atmosphere and ionosphere is greatly influenced by the complex
15   characteristics of the upper stratosphere, and the mesosphere and lower thermosphere (MLT). However, measurements of wind speeds are still lacking in these altitude regions, particularly between 30 and 60 km, which is also known as the "radar gap" (Shepherd, 2015).

    Mesosphere, Stratosphere, Thermosphere (MST) radar and meteor radar are typically used in ground-based observation to measure wind above 70 km or below 15 km (Blanc et al., 2018). The upper stratosphere and mesosphere can be measured
20   by Rayleigh-Mie Doppler wind lidar, but only under clear sky conditions (Yan et al., 2017). It has already been suggested to measure the Doppler frequency shift of microwave passive emission to retrieve the wind speed between 70 and 85 km altitude using the CO emission line at 230 GHz (Clancy and Muhleman, 1993). In 2007, a sub-millimeter telescope located in Antarctica at an altitude of 2847 m where the troposphere is very dry, was used to measure CO at 461 GHz to retrieve mesospheric mean winds (Burrows et al., 2007). The first ground-based microwave wind radiometer Wind Radiometer (WIRA)

25  and its successor Wind Radiometer for Campaigns (WIRA-C) have achieved to observe wind profiles between 35 and 75 km altitude for long-term stationary observations from 2012 (Ruefenacht et al., 2012; Rüfenacht et al., 2014; Hagen et al., 2018). In addition, ground-based observations in the 230–250 GHz $O_3$ and CO lines region were also studied in the previously research (Newnham et al., 2016).

The spaceborne interferometers such as Wind Imaging Interferometer (WINDII), Fabry–Perot High Resolution Doppler
30  Imager (HRDI), and TIMED Doppler Imager (TIDI) were designed to measure wind down to 85, 50 and 70 km, respectively (Gault et al., 1996; Burrage et al., 1996; Killeen et al., 2006). The Atmospheric Laser Doppler Instrument (ALADIN) onboard Aeolus satellite can measure wind below 30 km (Witschas et al., 2020). Using the 118 GHz $O_2$ line measured by microwave radiometer with a high-resolution spectrometer, Microwave Limb Sounder (MLS) onboard Aura satellite first achieved the space microwave measurement of atmospheric line-of-sight wind between 70 and 90 km (a precision of 17 m s$^{-1}$) (Wu et al.,
35  2008). By measuring the $O_3$ line and HCl line at 625 GHz band, the Superconducting Submillimeter-Wave Limb-Emission Sounder (SMILES) observed wind between 30 and 80 km, with the highest precision being 7-9 m s$^{-1}$ (Baron et al., 2013b). Its successor SMILES-2 has been proposed to the Japan Aerospace Exploration Agency (JAXA) and wind (30–110 km) is one of the main target parameters (expected precision: 2–5 m s$^{-1}$) (Ochiai et al., 2017; Baron et al., 2020). Another proposed payload is the Stratospheric Inferred Winds (SIW) instrument of the Swedish InnoSat program which has been selected for
40  launch in recent years (Baron et al., 2018). Its frequency is centered at 655 GHz and will provide horizontal wind vectors within 30–90 km. THz limb sounder (TLS) is a concept instrument for lower thermospheric neutral wind/density/temperature and can provide wind profiles of 100–180 km (Wu et al., 2016; Yee et al., 2021). A study described by Baron et al. (2013a) provides wind retrieval simulations from 100 GHz to 3 THz, with the bandwidth and the spectral resolution is 8 GHz and 1 MHz, respectively. The conclusion is that the line-of-sight wind can be derived from 25 to more than 90 km with a radiometer
45  of moderate sensitivity. The vertical resolution is better than 5 km and the precision is better than 10 m s$^{-1}$ in the middle and upper mesosphere (the precision is 2–3 m s$^{-1}$ from 40 to 65 km). However, investigations on the retrieval performance using a combination of different bands and the impact of instrument parameters were insufficient in the previous studies. In the context of the principal prototype: THz atmospheric limb sounder (TALIS) of China (Wang et al., 2020; Xu et al., 2022), atmospheric wind becomes a key target which needs to be considered in the band optimization of subsequent instrument development. This
50  study will provide reference for future payload design.

In this study, we present an optimal band selection analysis for measuring wind in terahertz (THz) frequency bands (0.1–5 THz). The sensitivity of atmospheric molecules to wind at different altitudes and the corresponding frequency bands is analyzed by using radiative transfer simulations. The requirements of spectral resolution, spectral bandwidth and radiometric measurement noise are also discussed. Different band combinations for middle and upper atmospheric wind measurement and the corre-
55  sponding payload parameters are compared at last. The article is organized as follows. The principle and method are briefly introduced in Sect. 2. The band pre-selection is explained in Sect. 3. Section 4 show the analysis of different instrument parameters. At last, Sect. 5 concludes the study.

## 2 Methodology

A radiometer with high-resolution spectrometers can measure the Doppler shift of spectral lines caused by the velocity of atmospheric gases with respect to the radiometer. Limb sounding is an effective method for measuring wind from space since the emission lines have a much greater signal-to-noise ratio (SNR) and sensitivity of wind than nadir observation. Figure 1 shows the wind measurement principle of a radiometer. Although the value of Doppler shift is small (typically less than 300 kHz) and is difficult to be measured directly due to the large noise at such a high spectral resolution, the variation of brightness temperature (BT) induced by wind is amplified by the spectral line broadening and can be detected ($\Delta T$ shown in Fig. 1). As the signature characteristics shown in Baron et al. (2013a), the wind signature is anti-symmetric with respect to the line rest frequency and the position of the maximum BT depends on the line shape but not on the Doppler shift. Therefore, the spectral resolution of measurement does not need to reach as high as 100 kHz and the retrieval problem can be solved by the linear least-squares method.

### 2.1 Retrieval method

The BT received by the radiometer can be calculated using radiative transfer theory. Neglecting scattering and assuming Local Thermodynamic Equilibrium (LTE), the formal solution of the radiative transfer equation is defined as (Urban, 2003):

$$I_v(S_2) = I_v(S_1)e^{-\int_{S_1}^{S_2} \alpha_v(s)ds} + \int_{S_1}^{S_2} \alpha_v(s)B_v(T)e^{-\int_{S_1}^{S_2} \alpha_v(s)ds}ds, \tag{1}$$

where $I_v$ is the radiance at frequency $v$ from position $S_1$ reaching the sensor $S_2$, $\alpha$ is the total absorption coefficient. $B_v(T)$ stands for the atmospheric emission which is given by the Planck function at temperature $T$.

The optimal estimation method (OEM) is employed as the retrieval algorithm (Rodgers, 2000). The cost function is given by:

$$\chi^2 = [y - \boldsymbol{F}(x,b)]^T \boldsymbol{S}_y^{-1}[y - \boldsymbol{F}(x,b)] + [x - x_a]^T \boldsymbol{S}_x^{-1}[x - x_a], \tag{2}$$

where $x_a$ is the a priori state vector, $\boldsymbol{S}_x$ and $\boldsymbol{S}_y$ are the covariance matrices representing the natural variability of the state vector and the measurement error vector, respectively. The retrieved state vector is given by:

$$x_{i+1} = x_a + (\boldsymbol{K}_x^T \boldsymbol{S}_y^{-1} \boldsymbol{K}_x + \boldsymbol{S}_x^{-1})^{-1}[y - \boldsymbol{F}(x,b) + \boldsymbol{K}_x(x_i - x_a)], \tag{3}$$

where $\boldsymbol{K}_x$ represents the Jacobian matrix of the radiative transfer model.

The retrieval precision can be described by two covariance matrices, the smoothing (or "null-space") error covariance matrix which is due to the a priori profile with an assumed error for regularization:

$$\boldsymbol{S}_n = (\boldsymbol{A} - \boldsymbol{I})\boldsymbol{S}_x(\boldsymbol{A} - \boldsymbol{I})^T, \tag{4}$$

$$\boldsymbol{A} = \boldsymbol{G}_y\boldsymbol{K}_x, \tag{5}$$

$$\boldsymbol{G}_y = (\boldsymbol{K}_x^T \boldsymbol{S}_y^{-1} \boldsymbol{K}_x + \boldsymbol{S}_x^{-1})^{-1}\boldsymbol{K}_x^T \boldsymbol{S}_y^{-1}, \tag{6}$$

Atmospheric
Measurement
Techniques
Discussions

and the measurement error covariance matrix due to the measurement noise:

$$\boldsymbol{S}_m = \boldsymbol{G}_y \boldsymbol{S}_y \boldsymbol{G}_y^T. \tag{7}$$

The precision in the following simulation is the total of $\boldsymbol{S}_n$ and $\boldsymbol{S}_m$:

$$\epsilon = \sqrt{diag(\boldsymbol{S}_n + \boldsymbol{S}_m)}. \tag{8}$$

## 3 Simulations of band selection

### 3.1 Pre-selection of target spectral bands

The spectroscopic lines of common atmospheric molecules in the THz band from the HITRAN-2016 database are used for the line-by-line calculation (Gordon et al., 2017). Since the brightness temperature is proportional to the molecule line intensity and volume mixing ratio (VMR), considering their strongest line and typical VMR in the Earth's atmosphere, the following molecules are selected for further analysis: $H_2O$, $O_3$, $CO$, $O_2$, HF, HCl and O atom (OI). The simulation atmospheric profiles are derived from the FASCOD standard database, i.e. Air Force Geophysics Laboratory (AFGL) model (Anderson et al., 1986). Profiles cover an altitude range of 0–120 km and include six typical scenarios (15°N, 45°N winter/summer, 60°N winter/summer and U.S. standard). Figure 2 shows the five temperature profiles from AFGL and the zonal mean wind profiles from the HWM14 model (Drob et al., 2015).

A simulation of the BT caused by Doppler shift from atmospheric wind is carried out using the Atmospheric Radiative Transfer Simulator (ARTS, v2.4.0) (Buehler et al., 2018). At a frequency interval of 5 MHz, the ΔBTs are simulated at tangent heights of 20, 30, 50, 70, 90 and 110 km. To prevent interpolation errors, the Doppler shift calculation is performed in the "on-the-fly" mode. Five typical profiles are used in the pre-selection simulation while only the result of the tropical profile is shown in Fig. 3. The others are calculated but not shown here. Different profiles lead to different ΔBTs, however, the central frequencies are similar.

The results in Fig. 3 demonstrated that BT induced by wind can be as large as 10 K and different molecules are sensitive to different altitudes. Although the BT variation (i.e. wind signal) becomes larger with increasing frequency, the system noise temperature also increases correspondingly. From the perspective of SNR, most of the high frequencies do not have better SNR than the low frequencies. The BT of wind at 50 km comes mainly from the numerous $O_3$ spectral lines, and the BT induced by wind at 70 km is significant at the $O_2$ and $H_2O$ spectral lines. Furthermore, wind can be obtained up to 90 km by strong spectral lines of $O_2$ and $H_2O$. Finally, BT of wind at 110 km exists only at two spectral lines of OI. Therefore, based on the above simulation results, the pre-selected central frequencies are listed in Table I.

### 3.2 Performance evaluation

The OEM retrieval is implemented by Qpack2 which uses ARTS as the forward model (Eriksson et al., 2005). Measurements are assumed to scan tangent height from 20 to 120 km at 600 km orbit and obtain the spectra every 1 km. Single sideband

Atmospheric
Measurement
Techniques
Discussions

(SSB) measurement is assumed in the whole study. The spectral bandwidth and resolution of radiometer in this simulation is 4 GHz and 1MHz. The system noise temperature for a double sideband (DSB) radiometer at ambient temperature can be simply calculated as a function of frequency (Hubers, 2008):

120 $$T_{sys} = 50 \times hF/k, \tag{9}$$

where the $h$ is Planck constant, $k$ is Boltzmann constant and $F$ is frequency. The measurement noise or noise equivalent delta temperature (NEDT) can be calculated as (Baron et al., 2013a):

$$NEDT(SSB) \approx 2 \times NEDT(DSB) = \frac{2 \times T_{sys}}{\sqrt{\beta d\tau}}, \tag{10}$$

where $\beta$ is the spectral resolution (Hz) and $d\tau$ is the integration time (s). The measurement noise can be decreased to half
125 when the radiometer mixer is cooling down to 100 K which is the assumption in the following simulation (i.e. NEDT multiplied by 0.5). More about the system noise temperature is discussed in Sec. 4.

Due to the purpose of channel selection, the a priori molecule profiles which will affect retrieval precision is not considered in this study. The a priori wind profile and corresponding covariance used for retrieval regularization are assumed to be 0 m s$^{-1}$ and 100 m s$^{-1}$, respectively. It should be noted that the Zeeman effect of $O_2$ and OI is not considered here, but it cannot
130 be ignored in real retrieval. Figures 4-8 show the performance of the different frequency bands in wind measurements of the tropical atmosphere.

According to the above retrieval results, it can be found that the effective range of the radiometer for measuring wind is mostly above 35 km, which may be due to the broadening of the spectral line in the lower atmosphere so that the Doppler signal is hidden in the broadening. Taking the error of 10 m s$^{-1}$ as the limit, the sensitive altitude range of $H_2O$ spectral lines is
135 45–100 km (see Fig. 4). The 448 and 556 GHz bands show the best performance at 70–80 km and 90–100 km respectively, and bands above 1 THz show poorer precision. The 474 and 620 GHz bands show a little better than 448 GHz at 50–70 km while the 620 GHz band become much poorer below 50 km. Figure 5 shows the results of $O_3$ bands which are sensitive to 40–85 km. All bands show very high precision at 50–70 km (better than $H_2O$ bands) and the 655 GHz band show the best performance for stratospheric wind measurement. Furthermore, the 840 GHz band also show good precision in this region and it is possible
140 to cover the 834 GHz $O_2$ line simultaneously to improve the performance at higher altitude. Figure 6 shows that $O_2$ bands are sensitive to 45–100 km which is similar to $H_2O$ bands. However, $O_2$ band perform better than $H_2O$ band at 70–90 km due to its constant VMR at higher altitude. The 118 and 487 GHz band shows best precision at this altitude range. The HCl, HF and CO bands show poorer precision compared to other bands (see Figs. 7-8). The OI spectral lines at 2.06 and 4.74 THz show good sensitivity to wind above 105 km which is due to the rapidly increasing VMR of OI in the thermosphere. OI is the
145 only molecule in the THz band that can be used to measure wind at this altitude. In addition, the $O_3$ lines near these center frequencies also provide information from the stratospheric wind.

Although there are averaging kernels larger than 0.5 at 30–40 km which means the wind is possible to be detected, the precision is poor due to too much small SNR. Thus, reducing system noise can improve retrieval precision in the lower stratosphere. Data averaging is also an useful way to obtain the high precision product at this altitude.

Atmospheric
Measurement
Techniques
Discussions
Open Access
EGU

150　For wind retrieval, line intensity and shape can both have an impact on $\Delta BT$. It means that not the stronger spectral line the higher precision, some less intense lines can also get the better precision. It is clear that a steep decrease from the spectral line center to line wings (i.e. narrow line width) is better for wind measurement. According to the results above, the potential frequency bands include: 118, 448, 487, 556, 655, 840 (broadband can simultaneously cover 834 GHz $O_2$ line) and 2060 GHz.

## 4　Analysis of instrumental parameters

### 4.1　Spectral resolution

155

Spectral resolution is an important instrument parameter since the Doppler shift from wind is usually small, high resolution can provide more complete spectrum information but lead to larger measurement noise. Thus, a trade-off between resolution and noise should be considered. Figures 9-15 show the wind retrieval performance assuming the bandwidth is 1 GHz and the spectral resolution is 0.5, 1, 2 and 4 MHz, respectively. Two cases of the same noise (i.e. noise from 0.5 MHz resolution) and

160　normal noise are compared. It is clear that the higher resolution, the better retrieval precision under the same noise conditions.

For the 118 GHz band shown in Fig. 9, 0.5 MHz resolution shows good performance at an altitude of 95–110 km while other resolutions are not sensitive to this range. This is because the narrow Doppler broadening of molecule lines above the stratosphere needs a finer resolution to detect the shift caused by wind. Although 2 MHz resolution shows the best precision below 80 km, the difference is quite small. The effect of resolution is small at the 448 GHz band, and 2 MHz resolution is the

165　best (see Fig. 10). For the 487 GHz band, 0.5, 1 and 2 MHz resolution has similar performance while 4 MHz resolution has a large precision decrease at 60–80 km which means that this resolution will miss some important spectral line information. Results in Fig. 11 show that 2 MHz resolution is relatively good at the 487 GHz band. The 556 GHz band is sensitive to 70–100 km when the resolution is smaller than 1 MHz, and the 0.5 MHz resolution performs best (see Fig. 12). Results of 655 and 840 GHz band in Figs. 13-14 show that 1 MHz resolution is best for $O_3$ lines and finer resolution does not bring great

170　improvement, but rather reduces the precision in the upper atmosphere. Figure 15 shows that different resolutions have similar precision at the 2060 GHz band above 105 km, and the 2 MHz resolution is finally selected.

### 4.2　Spectral bandwidth

In the upper atmosphere, the Doppler broadening is narrow which indicates that fine spectral resolution is needed as discussed above, while in the lower atmosphere, the large pressure broadening may require a large spectral bandwidth. Figures 16-19

175　show the wind retrieval performance assuming the resolution is 4 MHz and the spectral bandwidth is 1, 2, 4 and 8 GHz, respectively.

Figure 16 (a) shows the results of two $O_2$ bands, since there are no other strong lines near the 118 GHz band, bandwidth has no impact on the results. From Fig. 16 (b), it can be found the larger bandwidth improves precision of 487 GHz band below 80 km. The same conclusion can also be applied to other bands due to the fact that large bandwidth may cover more

180　$O_3$ lines, which provide more wind signals in the lower atmosphere. For the 448 GHz band shown in Fig. 17 (a), increasing

Atmospheric
Measurement
Techniques
Discussions

Open Access

EGU

bandwidth improves the precision below 70 km and 4 GHz bandwidth is enough. Fig. 17 (b) shows an 8 GHz bandwidth can significantly improve the retrieval precision below 70 km at the 556 GHz band. Nevertheless, $O_3$ bands are more appropriate for wind measurement below 70 km. From this perspective, combination with $O_3$ band is a better choice and 2 GHz bandwidth for the $H_2O$ band is sufficient to measure wind at 70–80 km. For the $O_3$ bands depicted in Fig. 18, increasing the bandwidth

185 can significantly improve the retrieval precision. Although 4 GHz bandwidth is enough for an altitude above 50 km at 655 GHz band, 8 GHz can give more information below. Just as the case given by Baron et alBaron et al. (2013a), the best retrieval results (better than 15 m s$^{-1}$) can be obtained at 25 km using 16 GHz bandwidth at 359 GHz band. It should be noted that an 8 GHz bandwidth of the 840 GHz band can cover the $O_2$ line at 834 GHz which improves the precision a lot above 70 km. Moreover, large bandwidth is no need to be considered at the 2060 GHz band because this band is only used for wind measurements above

190 100 km.

According to the simulations above, there are four combinations of different bands selected for atmospheric wind measurement from 0–120 km: 1) 837.5 and 2060.07 GHz; 2) 487.25, 655 and 2060.07 GHz; 3) 118.75, 655 and 2060.07 GHz; 4) 118.75, 448, 655 and 2060.07 GHz. The corresponding parameters are listed in Table II.

### 4.3  System noise temperature

195 The measurement noise induced by receivers is the main error source in OEM retrieval. System noise temperature and NEDT can be calculated according to the (9) and (10). As stated above, NEDT has a direct impact on measurement precision. This section focuses on the comparison of three different noise cases which is achieved by multiplying the NEDT by different factors shown in Table II: 1) the radiometer cooled to 100 K (factor is 0.5); 2) the radiometer at ambient temperature (factor is 1); 3) the radiometer with larger noise temperature (factor is 2). The four band combinations discussed above are used in the

200 following simulations.

Figure 20 shows the performance evaluations of the four band combinations with three different noises. It is clear that retrieval error increases with the increase of NEDT. Comparing the different NEDT cases, the radiometer cooled to 100 K (i.e. NEDT with factor 0.5) shows the best performance and the precision can be better than 5 m s$^{-1}$ in most stratospheric and mesospheric regions and the best precision is about 1 m s$^{-1}$ at 60 and 100 km. The result of the normal case (i.e. NEDT with

205 factor 1) demonstrates that it is feasible to use a THz radiometer for limb sounding the middle and upper atmospheric wind. The precision in most target altitudes can be better than 10 m s$^{-1}$ and as good as about 3 m s$^{-1}$ at 60 and 100 km. The result of the noisy case (i.e. NEDT with factor 2) is poor but also shows acceptable precision (better than 15 m s$^{-1}$) from 50 to 100 km.

Considering the case where the NEDT factor is 1 (red line in Fig. 20), Combination 1 shows the poorest precision especially when altitude is above 70 km since the weak $O_2$ line at 834 GHz cannot provide sufficient sensitivity to wind at this region.

210 However, with a 10 m s$^{-1}$ error limit, this combination can still measure wind from 45 to about 90 km. The precision is better than 5 m s$^{-1}$ at 50–65 km and about 7 m s$^{-1}$ at 70–85 km. The advantage of Combination 1 is the lowest cost of bands. Combination 2 uses the 487.25 GHz $O_2$ line and 655 GHz $O_3$ lines instead of the 840 GHz band to enhance the line intensity and reduce the measurement noise for better performance. The precision is better than 6 m s$^{-1}$ from 50 to 95 km. Combination 3 replaces the 487.25 GHz $O_2$ line with 118.75 GHz, further improving the measurement performance above

215   90 km and increasing the effective altitude to 110 km from 90–100 km in the first two combinations. The precision can be better than 6 m s$^{-1}$ from 50 to 105 km. Although the 118 GHz band has better performance than the 487 GHz band, the disadvantage of this combination is that the 118 GHz radiometer needs a larger antenna and has a lower vertical resolution. Combination 4 adds an extra 448 GHz band to improve the performance at 60–80 km. Comparing the results of Combination 3 and Combination 4, the retrieval precision of 60–80 km has indeed improved, but the improvement is not significant ($\sim 1$ m

220   s$^{-1}$). Whether a new band is needed to improve a little precision still needs to be considered.

## 5   Conclusions

In this study, simulations of atmospheric wind measurement using a THz limb sounder are performed using radiative transfer model ARTS. The target molecules and corresponding optimal frequencies in the THz band are also analyzed. By comparing the results, $H_2O$, $O_3$, $O_2$ and OI are selected since their spectral lines have good sensitivity to different altitude wind. Although

225   CO, HF and HCl can also provide wind information, their retrieval precision is relatively poor. By combining the best bands of $H_2O$, $O_3$, $O_2$ and OI, good wind measurement (total precision is better than 10 m s$^{-1}$ and best precision is 1 m s$^{-1}$) can be performed over 40–120 km. The 118, 448, 487, 655, 837 and 2060 GHz frequency bands are the final selected for atmospheric wind observation and four combinations are compared for different advantages and disadvantages.

Spectral bandwidth, resolution and NEDT of receiver are the main instrument parameters for radiometric measurement.

230   Due to the spectral line broadening effect, the wind signal is quite weak compared to the linewidth in the lower atmosphere (below 35 km), increasing bandwidth to cover more lines and decreasing NEDT both help improving the retrieval precision. The results show that $O_3$ bands are sensitive to the stratospheric wind which need large bandwidth (4–8 GHz) while the other molecules sensitive to MLT doesn't. Although Doppler wind measurement requires finer spectral resolution, only the 118 GHz band can derive a very significant performance improvement at 0.5 MHz resolution due to the negative relationship between

235   resolution and NEDT. With the current considered instrument noise, 1–2 MHz resolution is sufficient unless the radiometer is cooled down to 4 K. From the simulation results, it is obvious that the radiometer cooled down to 100 K or even to 4 K is very important for the high precision observation of upper atmospheric wind. At last, due to the lack of past and future wind observations in the middle and upper atmosphere, using a THz radiometer to fill the needs is a feasible and superior method.

*Author contributions.*   All authors designed the study. WW set up the retrieval experiments, analyzed the retrieval results, and wrote the article. JX provided guidance and insight regarding experiment configurations and results analysis. ZW revised the article.

*Competing interests.* Some authors are members of the editorial board of AMT. The peer-review process was guided by an independent editor, and the authors have also no other competing interests to declare.

Atmospheric
Measurement
Techniques
Discussions

# References

Anderson, G. P., Chetwynd, J. H., and She, E. P.: AFGL Atmospheric Constituent Profiles (0-120km), Air Force Geophys. Lab., Hanscom AFB, MA, afgl-tr-86-0110 edn., 1986.

250 Baldwin, M. P. and Dunkerton, T. J.: Stratospheric Harbingers of Anomalous Weather Regimes, Science, 294, 581–584, https://doi.org/10.1126/science.1063315, 2001.

Baldwin, M. P., Stephenson, D. B., Thompson, D. W. J., Dunkerton, T. J., Charlton, A. J., and O'Neill, A.: Stratospheric Memory and Skill of Extended-Range Weather Forecasts, Science, 301, 636–640, https://doi.org/10.1126/science.1087143, 2003.

Baron, P., Murtagh, D. P., Urban, J., Sagawa, H., Eriksson, P., and Ochiai, S.: Definition Of An Uncooled Submillimeter/Terahertz LIMB
255 Sounder For Measuring Middle Atmospheric Winds, in: Proc. ESA Living Planet Symposium 2013, pp. 1–8, Edinburgh, 2013a.

Baron, P., Murtagh, D. P., Urban, J., Sagawa, H., Ochiai, S., Kasai, Y., Kikuchi, K., Khosrawi, F., Kornich, H., Mizobuchi, S., Sagi, K., and Yasui, M.: Observation of horizontal winds in the middle-atmosphere between 30 degrees S and 55 degrees N during the northern winter 2009-2010, Atmos. Chem. Phys., 13, 6049–6064, https://doi.org/10.5194/acp-13-6049-2013, 2013b.

Baron, P., Murtagh, D., Eriksson, P., Mendrok, J., Ochiai, S., Perot, K., Sagawa, H., and Suzuki, M.: Simulation study for the Stratospheric In-
260 ferred Winds (SIW) sub-millimeter limb sounder, Atmos. Meas. Tech., 11, 4545–4566, https://doi.org/10.5194/amt-11-4545-2018, 2018.

Baron, P., Ochiai, S., Dupuy, E., Larsson, R., Liu, H., Manago, N., Murtagh, D., Oyama, S.-i., Sagawa, H., Saito, A., Sakazaki, T., Shiotani, M., and Suzuki, M.: Potential for the measurement of mesosphere and lower thermosphere (MLT) wind, temperature, density and ge-omagnetic field with Superconducting Submillimeter-Wave Limb-Emission Sounder 2 (SMILES-2), Atmos. Meas. Tech., 13, 219–237, https://doi.org/10.5194/amt-13-219-2020, 2020.

265 Blanc, E., Ceranna, L., Hauchecorne, A., Charlton-Perez, A., Marchetti, E., Evers, L. G., Kvaerna, T., Lastovicka, J., Eliasson, L., Crosby, N. B., Blanc-Benon, P., Le Pichon, A., Brachet, N., Pilger, C., Keckhut, P., Assink, J. D., Smets, P. S. M., Lee, C. F., Kero, J., Sindelarova, T., Kämpfer, N., Rüfenacht, R., Farges, T., Millet, C., Näsholm, S. P., Gibbons, S. J., Espy, P. J., Hibbins, R. E., Heinrich, P., Ripepe, M., Khaykin, S., Mze, N., and Chum, J.: Toward an Improved Representation of Middle Atmospheric Dynamics Thanks to the ARISE Project, Surv. Geophys., 39, 171–225, https://doi.org/10.1007/s10712-017-9444-0, 2018.

270 Buehler, S. A., Mendrok, J., Eriksson, P., Perrin, A., Larsson, R., and Lemke, O.: ARTS, the Atmospheric Radiative Transfer Simulator - version 2.2, the planetary toolbox edition, Geosci. Model Dev., 11, 1537–1556, https://doi.org/10.5194/gmd-11-1537-2018, 2018.

Burrage, M. D., Skinner, W. R., Gell, D. A., Hays, P. B., Marshall, A. R., Ortland, D. A., Manson, A. H., Franke, S. J., Fritts, D. C., Hoffman, P., McLandress, C., Niciejewski, R., Schmidlin, F. J., Shepherd, G. G., Singer, W., Tsuda, T., and Vincent, R. A.: Validation of mesosphere and lower thermosphere winds from the high resolution Doppler imager on UARS, J. Geophys. Res.-Atmos., 101, 10 365–
275 10 392, https://doi.org/10.1029/95JD01700, 1996.

Burrows, S. M., Martin, C. L., and Roberts, E. A.: High-latitude remote sensing of mesospheric wind speeds and carbon monoxide, J. Geophys. Res.-Atmos., 112, D17 109, https://doi.org/10.1029/2006JD007993, 2007.

Clancy, R. T. and Muhleman, D. O.: Groundbased Microwave Spectroscopy of the Earth's Stratosphere and Mesosphere, in: Atmospheric remote sensing by microwave radiometry, edited by Janssen, M. A., chap. 7, p. 372–374, Wiley-Interscience, New York, USA, 1993.

280 Drob, D. P., Emmert, J. T., Meriwether, J. W., Makela, J. J., Doornbos, E., Conde, M., Hernandez, G., Noto, J., Zawdie, K. A., McDonald, S. E., Huba, J. D., and Klenzing, J. H.: An update to the Horizontal Wind Model (HWM): The quiet time thermosphere, Earth Space Sci., 2, 301–319, https://doi.org/10.1002/2014EA000089, 2015.

Eriksson, P., Jimenez, C., and Buehler, S. A.: Qpack, a general tool for instrument simulation and retrieval work, J. Quant. Spectrosc. Radiat. Transf., 91, 47–64, https://doi.org/10.1016/j.jqsrt.2004.05.050, 2005.

285 Gault, W. A., Thuillier, G., Shepherd, G. G., Zhang, S. P., Wiens, R. H., Ward, W. E., Tai, C., Solheim, B. H., Rochon, Y. J., McLandress, C., Lathuillere, C., Fauliot, V., Hersé, M., Hersom, C. H., Gattinger, R., Bourg, L., Burrage, M. D., Franke, S. J., Hernandez, G., Manson, A., Niciejewski, R., and Vincent, R. A.: Validation of O($^1$ S) wind measurements by WINDII: the WIND Imaging Interferometer on UARS, J. Geophys. Res.-Atmos., 101, 10 405–10 430, https://doi.org/10.1029/95JD03352, 1996.

Gordon, I. E., Rothman, L. S., Hill, C., Kochanov, R. V., Tan, Y., Bernath, P. F., Birk, M., Boudon, V., Campargue, A., Chance, K. V., Drouin,
290 B. J., Flaud, J. M., Gamache, R. R., Hodges, J. T., Jacquemart, D., Perevalov, V. I., Perrin, A., Shine, K. P., Smith, M. A. H., Tennyson, J., Toon, G. C., Tran, H., Tyuterev, V. G., Barbe, A., Csaszar, A. G., Devi, V. M., Furtenbacher, T., Harrison, J. J., Hartmann, J. M., Jolly, A., Johnson, T. J., Karman, T., Kleiner, I., Kyuberis, A. A., Loos, J., Lyulin, O. M., Massie, S. T., Mikhailenko, S. N., Moazzen-Ahmadi, N., Mueller, H. S. P., Naumenko, O. V., Nikitin, A. V., Polyansky, O. L., Rey, M., Rotger, M., Sharpe, S. W., Sung, K., Starikova, E., Tashkun, S. A., Vander Auwera, J., Wagner, G., Wilzewski, J., Wcislo, P., Yu, S., and Zak, E. J.: The HITRAN2016 molecular spectroscopic
295 database, J. Quant. Spectrosc. Radiat. Transf., 203, 3–69, https://doi.org/10.1016/j.jqsrt.2017.06.038, 2017.

Hagen, J., Murk, A., Rüfenacht, R., Khaykin, S., Hauchecorne, A., and Kämpfer, N.: WIRA-C: a compact 142-GHz-radiometer for continuous middle-atmospheric wind measurements, Atmos. Meas. Tech., 11, 5007–5024, https://doi.org/10.5194/amt-11-5007-2018, 2018.

Hardiman, S. C., Butchart, N., Charlton-Perez, A. J., Shaw, T. A., Akiyoshi, H., Baumgaertner, A., Bekki, S., Braesicke, P., Chipperfield, M., Dameris, M., Garcia, R. R., Michou, M., Pawson, S., Rozanov, E., and Shibata, K.: Improved predictability of the troposphere using
300 stratospheric final warmings, J. Geophys. Res.-Atmos., 116, D18 113, https://doi.org/10.1029/2011JD015914, 2011.

Hubers, H.-W.: Terahertz Heterodyne Receivers, IEEE J. Sel. Top. Quantum Electron., 14, 378–391, https://doi.org/10.1109/JSTQE.2007.913964, 2008.

Killeen, T. L., Wu, Q., Solomon, S. C., Ortland, D. A., Skinner, W. R., Niciejewski, R. J., and Gell, D. A.: TIMED Doppler interferometer: Overview and recent results, Journal of Geophysical Research-Space Physics, 111, https://doi.org/10.1029/2005ja011484, 2006.

305 Newnham, D. A., Ford, G. P., Moffat-Griffin, T., and Pumphrey, H. C.: Simulation study for measurement of horizontal wind profiles in the polar stratosphere and mesosphere using ground-based observations of ozone and carbon monoxide lines in the 230–250 GHz region, Atmos. Meas. Tech., 9, 3309–3323, https://doi.org/10.5194/amt-9-3309-2016, 2016.

Ochiai, S., Baron, P., Nishibori, T., Irimajiri, Y., Uzawa, Y., Manabe, T., Maezawa, H., Mizuno, A., Nagahama, T., Sagawa, H., Suzuki, M., and Shiotani, M.: SMILES-2 Mission for Temperature, Wind, and Composition in the Whole Atmosphere, Sola, 13A, 13–18,
310 https://doi.org/10.2151/sola.13A-003, 2017.

Rodgers, C. D.: Inverse methods for atmospheric sounding: theory and practice, vol. 2, World scientific, Singapore, 2000.

Ruefenacht, R., Kaempfer, N., and Murk, A.: First middle-atmospheric zonal wind profile measurements with a new ground-based microwave Doppler-spectro-radiometer, Atmos. Meas. Tech., 5, 2647–2659, https://doi.org/10.5194/amt-5-2647-2012, 2012.

Rüfenacht, R., Murk, A., Kämpfer, N., Eriksson, P., and Buehler, S. A.: Middle-atmospheric zonal and meridional wind profiles from
315 polar, tropical and midlatitudes with the ground-based microwave Doppler wind radiometer WIRA, Atmos. Meas. Tech., 7, 4491–4505, https://doi.org/10.5194/amt-7-4491-2014, 2014.

Shepherd, G. G.: Development of wind measurement systems for future space missions, Acta Astronaut., 115, 206–217, https://doi.org/10.1016/j.actaastro.2015.05.015, 2015.

Urban, J.: Optimal sub-millimeter bands for passive limb observations of stratospheric HBr, BrO, HOCl, and HO2 from space, J. Quant.
320 Spectrosc. Radiat. Transf., 76, 145–178, https://doi.org/10.1016/s0022-4073(02)00051-1, 2003.

Wang, W., Wang, Z., and Duan, Y.: Performance evaluation of THz Atmospheric Limb Sounder (TALIS) of China, Atmos. Meas. Tech., 13, 13–38, https://doi.org/10.5194/amt-13-13-2020, 2020.

Witschas, B., Lemmerz, C., Geiß, A., Lux, O., Marksteiner, U., Rahm, S., Reitebuch, O., and Weiler, F.: First validation of Aeolus wind observations by airborne Doppler wind lidar measurements, Atmospheric Measurement Techniques, 13, 2381–2396, https://doi.org/10.5194/amt-13-2381-2020, 2020.

Wu, D. L., Schwartz, M. J., Waters, J. W., Limpasuvan, V., Wu, Q., and Killeen, T. L.: Mesospheric doppler wind measurements from Aura Microwave Limb Sounder (MLS), Adv. Space Res., 42, 1246–1252, https://doi.org/10.1016/j.asr.2007.06.014, 2008.

Wu, D. L., Yee, J.-H., Schlecht, E., Mehdi, I., Siles, J., and Drouin, B. J.: THz limb sounder (TLS) for lower thermospheric wind, oxygen density, and temperature, J. Geophys. Res-Space Phys., 121, 7301–7315, https://doi.org/10.1002/2015ja022314, 2016.

Xu, H., Lu, H., Wang, Z., Liu, J., and Wang, W.: The System Design and Preliminary Tests of the THz Atmospheric Limb Sounder (TALIS), IEEE Trans. Instrum. Meas., 71, 1–12, https://doi.org/10.1109/TIM.2021.3135008, 2022.

Yan, Z., Hu, X., Guo, W., Guo, S., Cheng, Y., Gong, J., and Yue, J.: Development of a mobile Doppler lidar system for wind and temperature measurements at 30–70 km, J. Quant. Spectrosc. Radiat. Transf., 188, 52–59, https://doi.org/10.1016/j.jqsrt.2016.04.024, 2017.

Yee, J.-H., Mehdi, I., Hayton, D., Siles, J., and Wu, D.: Remote Sensing of Global Lower Thermospheric Winds: Sensing Techniques and Sensor Design, in: Space Physics and Aeronomy, Upper Atmosphere Dynamics and Energetics, edited by Wang, W., Zhang, Y., and Paxton, L. J., vol. 4, chap. 22, p. 469–486, Wiley, Hoboken, NJ, USA, 2021.

**Table 1.** Molecules and emission line frequencies for wind measurement

| Molecule | Central Frequency (GHz) |
|---|---|
| $H_2O$ | 183.31, 448, 474.69, 556.93, 620.7, 916.2, 987.93, 1113.34, 1136.7, 1541.97, 1794.79, 2040.47, 2074.43, 3953.48 |
| $O_3$ | 359, 469, 481.62, 655, 695, 754.46, 840, 866.1, 895.1, 908.7, 1028, 1212, 1396, 1580, 1760, 1943, 2140, 2496, 2651, 2824 |
| CO | 806.65, 1036.91 |
| $O_2$ | 118.75, 487.25, 566.9, 715.39, 731.18, 1058.72, 1061.12, 1406.37, 1466.81, 1525.131, 1711.977, 1812.405, 2214.55, 2502.32, 2846.62, 3190.41, 3469.55, 3811.67, 3930.48, 4153.16, 4271.98, 4900.32 |
| HF | 1232.48, 3691.33 |
| HCl | 625.92, 1251.45, 1876.23, 3121.99, 3736.61, 3742.22, 4353.66, 4360.18, 4975.50 |
| OI | 2060.07, 4744.78 |

**Table 2.** Simulation parameters for different selected bands

| Central Frequency (GHz) | Bandwidth (GHz) | Resolution (MHz) | NEDT (K) Factor: 0.5/1/2 |
|---|---|---|---|
| 118.75 | 1 | 0.5 | 0.57/1.13/2.27 |
| 448 | 2 | 2 | 1.08/2.15/4.30 |
| 487.25 | 1 | 2 | 1.17/2.34/4.67 |
| 655 | 8 | 1 | 2.22/4.45/8.89 |
| 837.5 | 8 | 2 | 2.02/4.03/8.06 |
| 2060.07 | 1 | 2 | 4.94/9.89/19.77 |
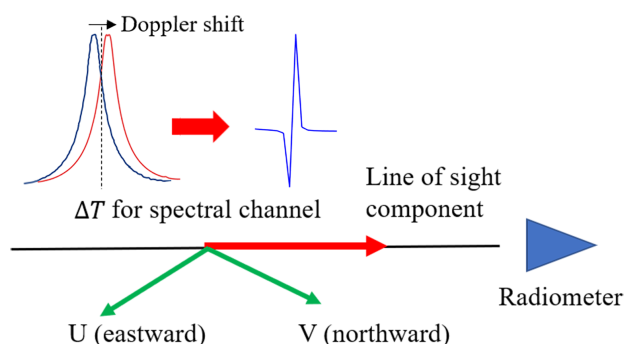


**Figure 1.** Principle of limb sounding of line-of-sight wind.
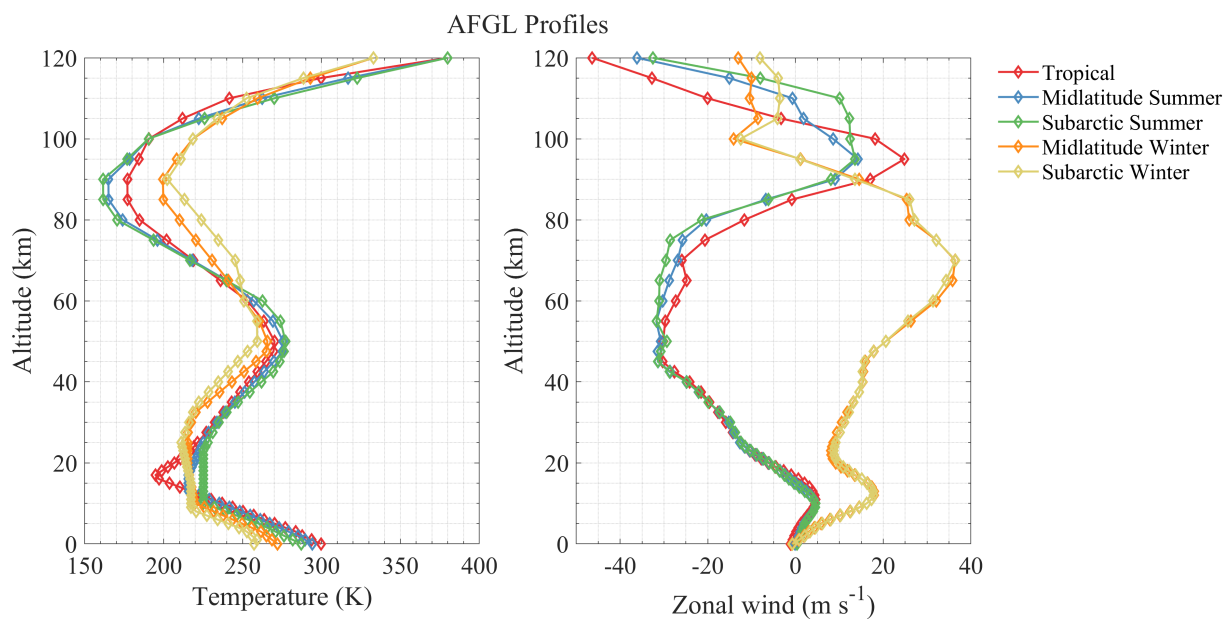
**Figure 2.** Temperature and wind profiles used in simulations.
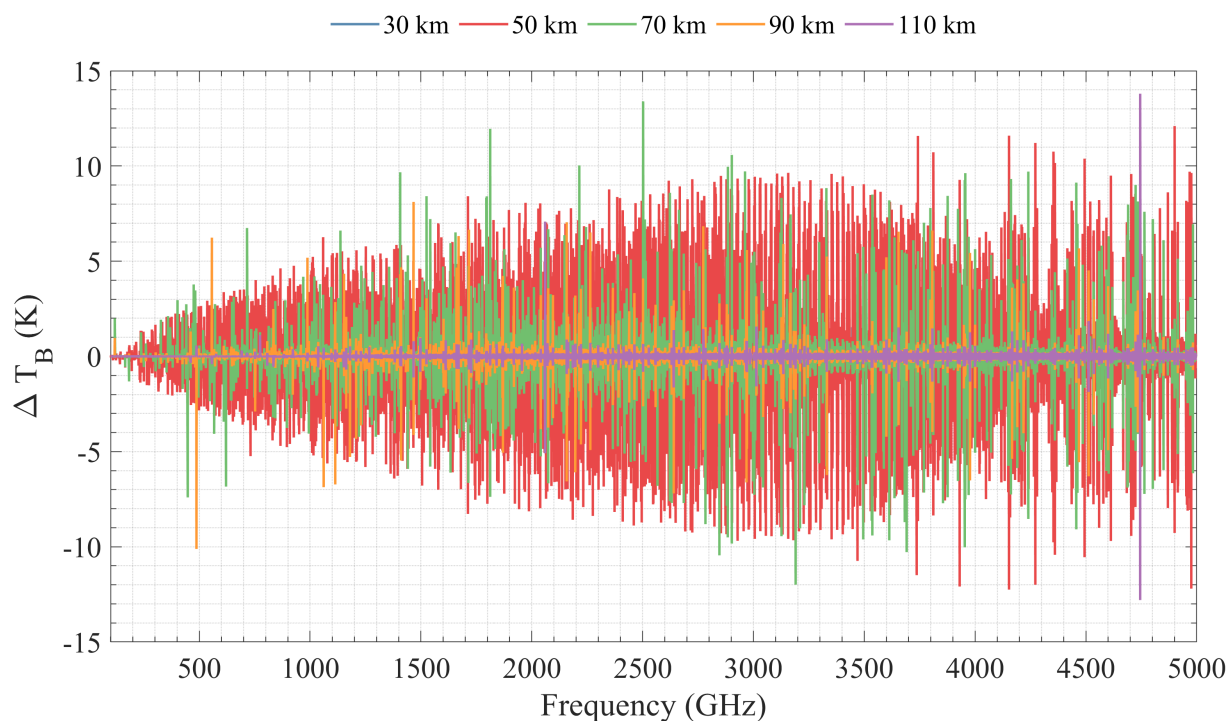


**Figure 3.** ΔBT induced by the wind for tropical profile.
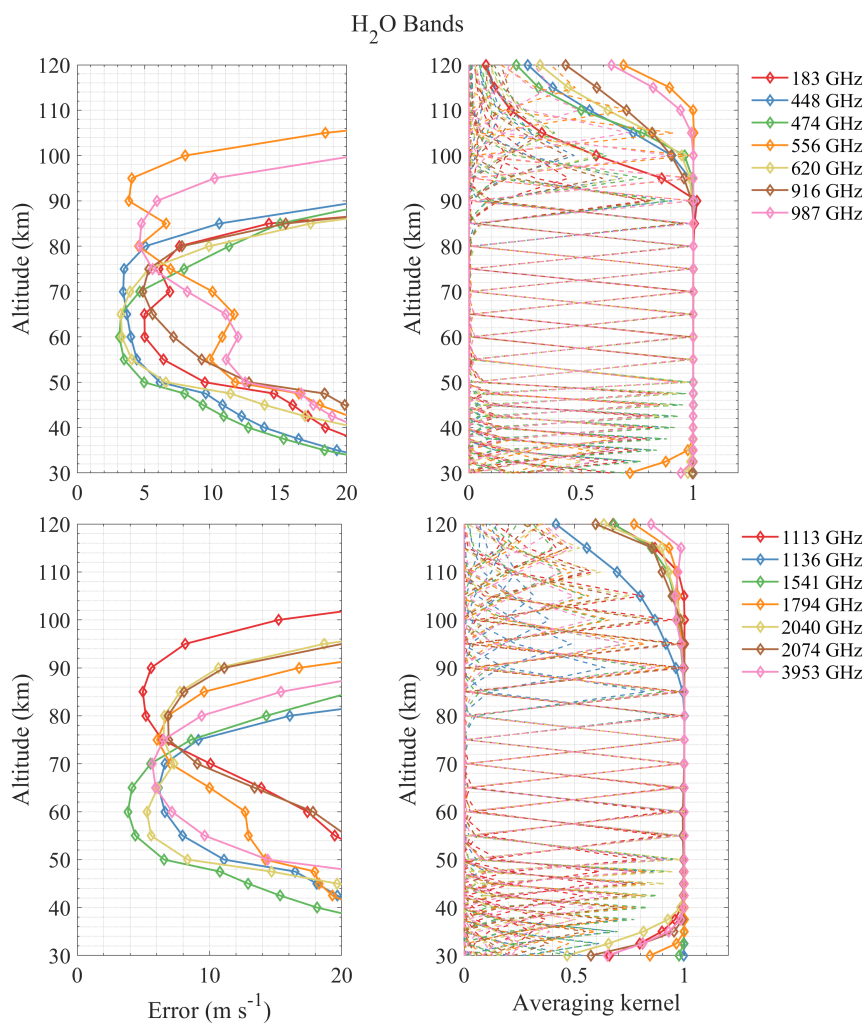
**Figure 4.** Results of wind retrieval using $H_2O$ bands.
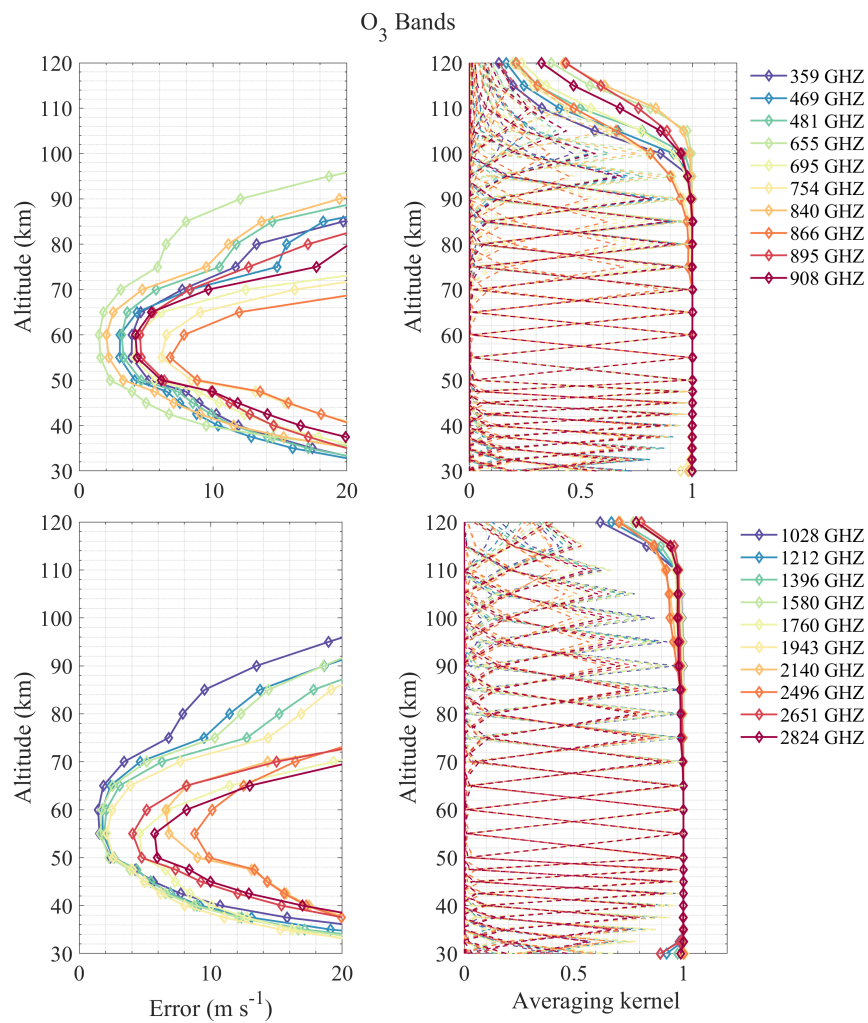
**Figure 5.** Same as Fig. 4 but for $O_3$ bands.
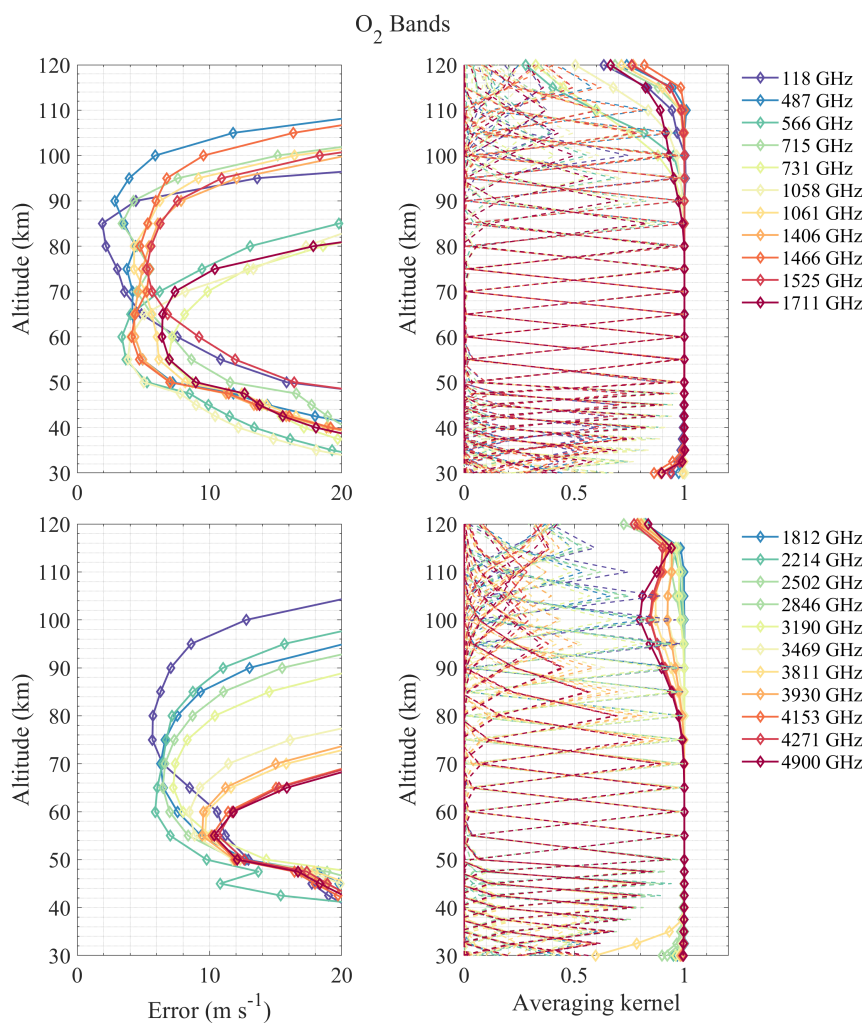
**Figure 6.** Same as Fig. 4 but for $O_2$ bands.

Atmospheric
Measurement
Techniques
Open Access
Discussions
EGU
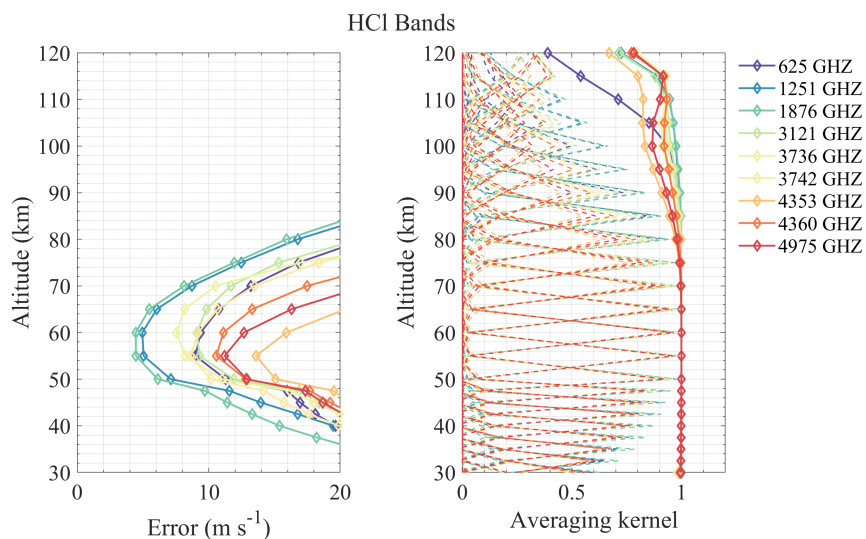


**Figure 7.** Same as Fig. 4 but for HCl bands.
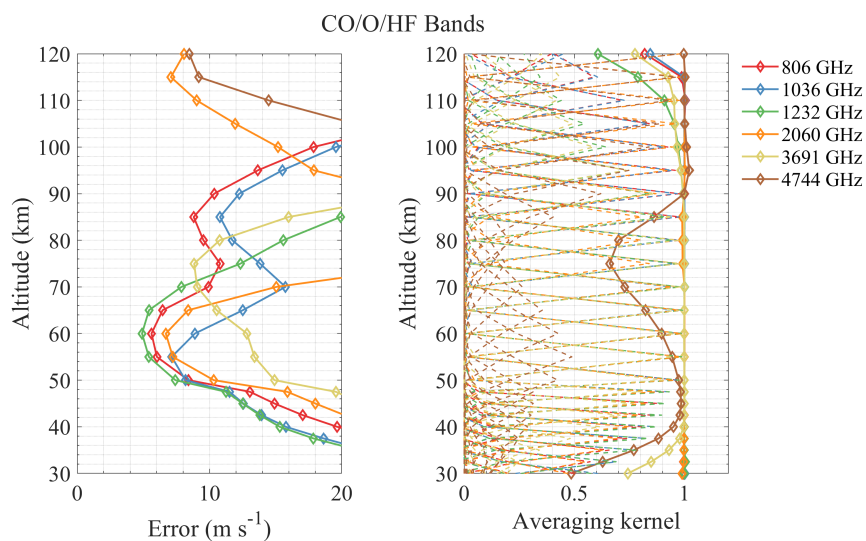


**Figure 8.** Same as Fig. 4 but for CO (806, 1036 GHz), HF (1232, 3691 GHz) and O (2060, 4744 GHz) bands.
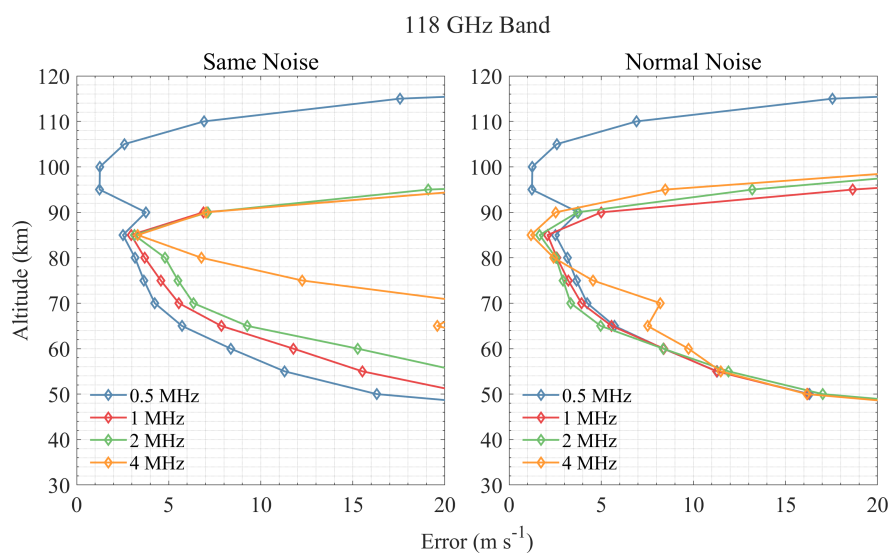
**Figure 9.** Performance comparison of different spectral resolutions of the 118 GHz band.
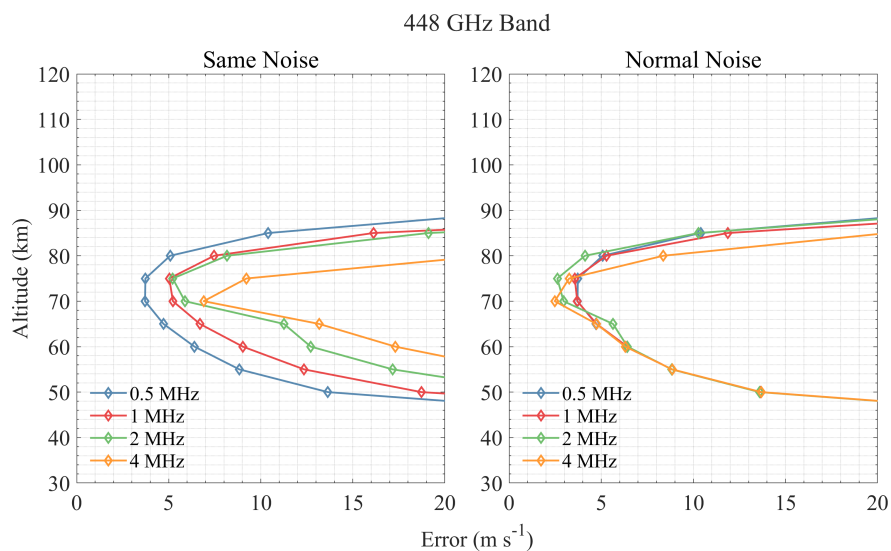


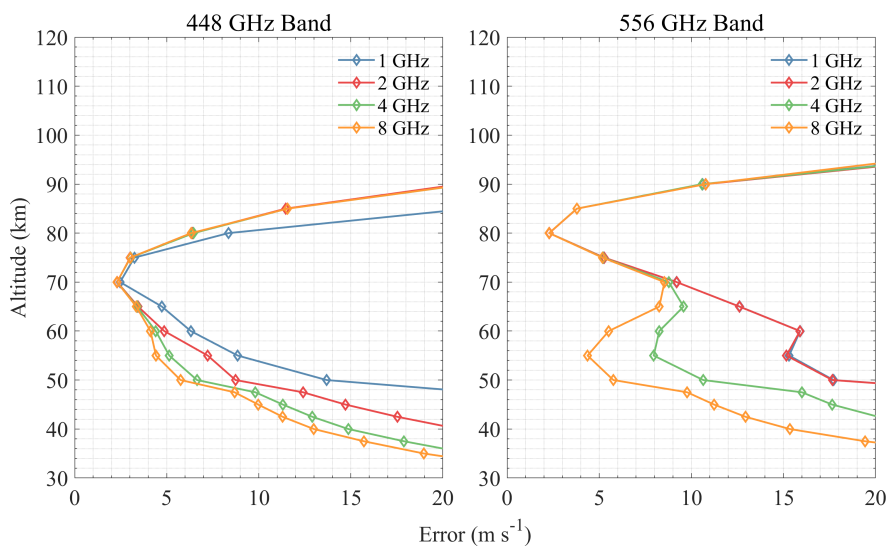**Figure 10.** Same as Fig. 9 but for the 448 GHz band.
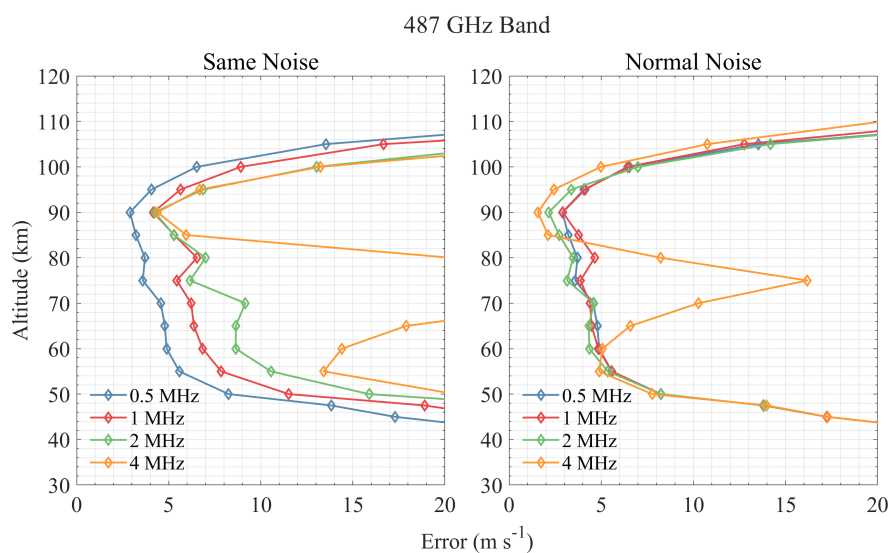
**Figure 11.** Same as Fig. 9 but for the 487 GHz band.
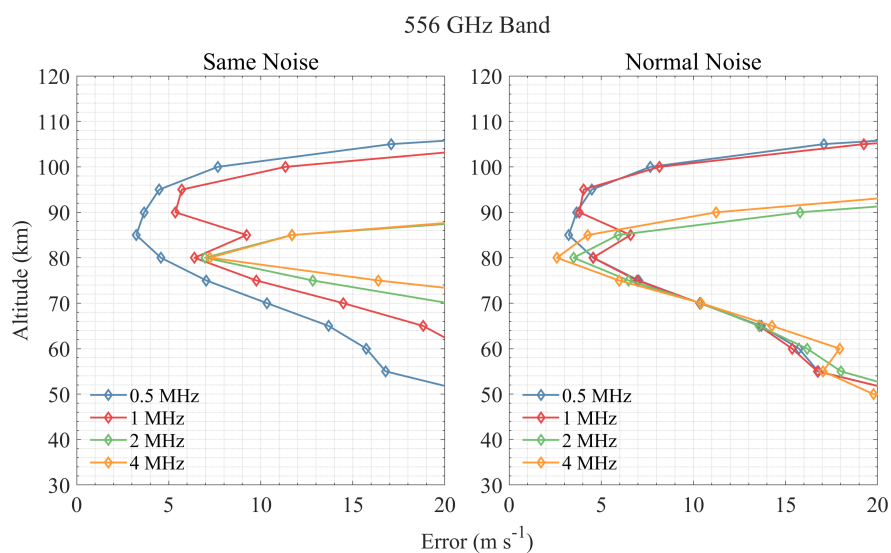


**Figure 12.** Same as Fig. 9 but for the 556 GHz band.
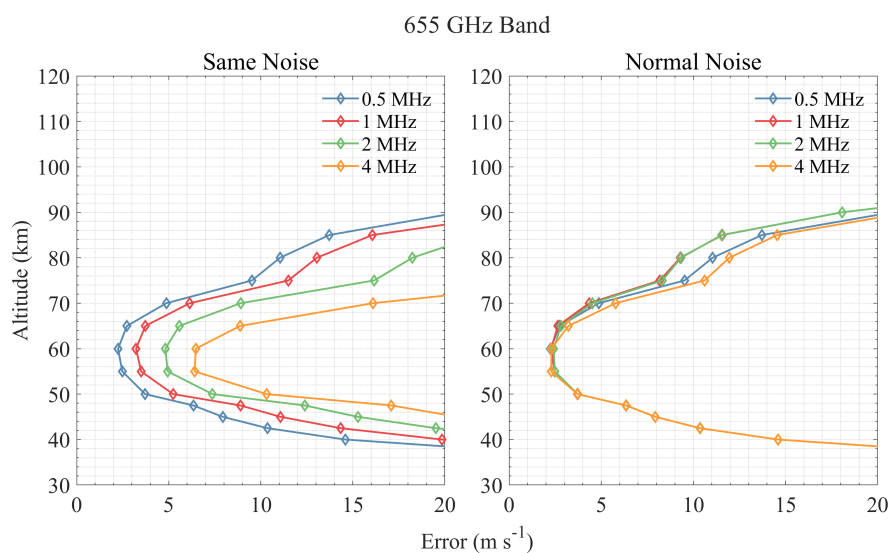
**Figure 13.** Same as Fig. 9 but for the 655 GHz band.
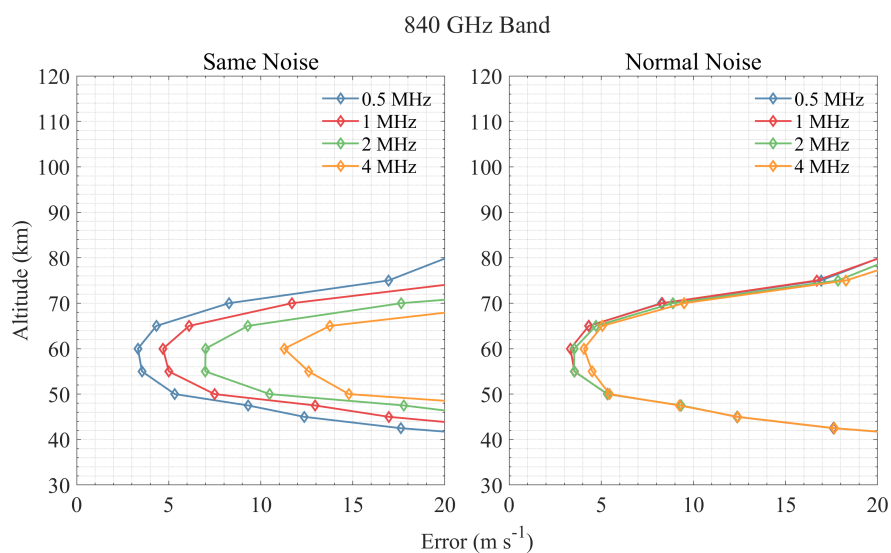


**Figure 14.** Same as Fig. 9 but for the 840 GHz band.
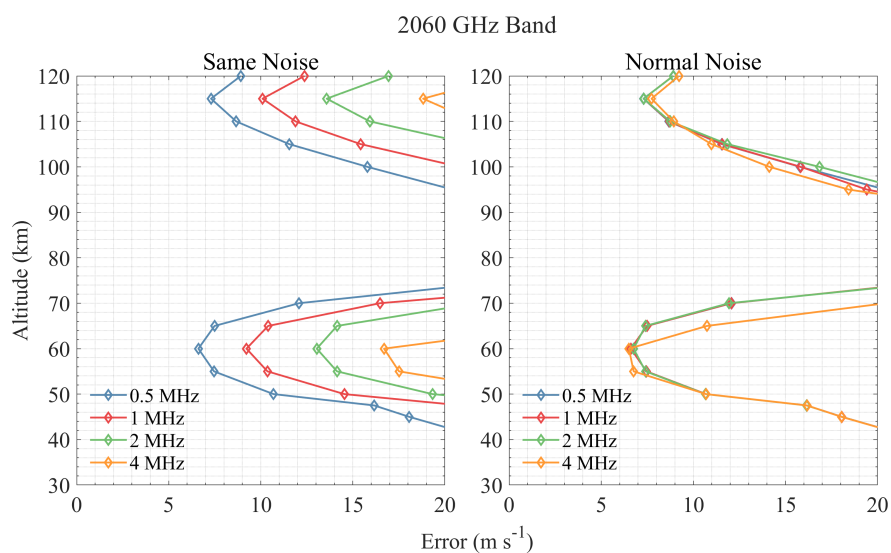
**Figure 15.** Same as Fig. 9 but for the 2060 GHz band.
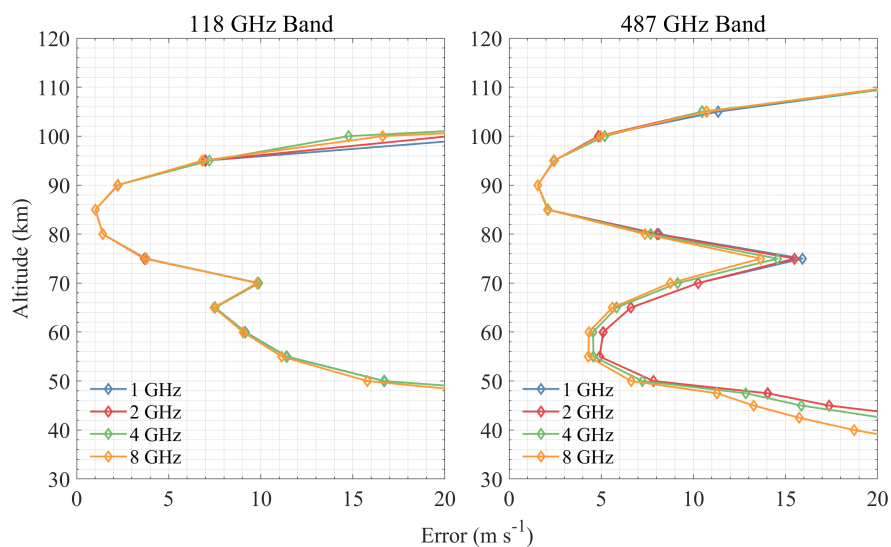


**Figure 16.** Performance comparison of different spectral bandwidths of the 118 and 487 GHz band.

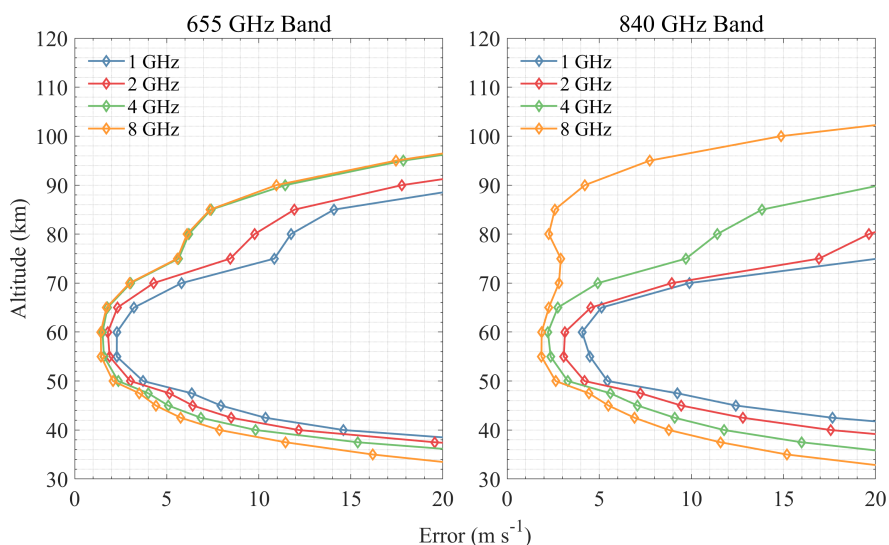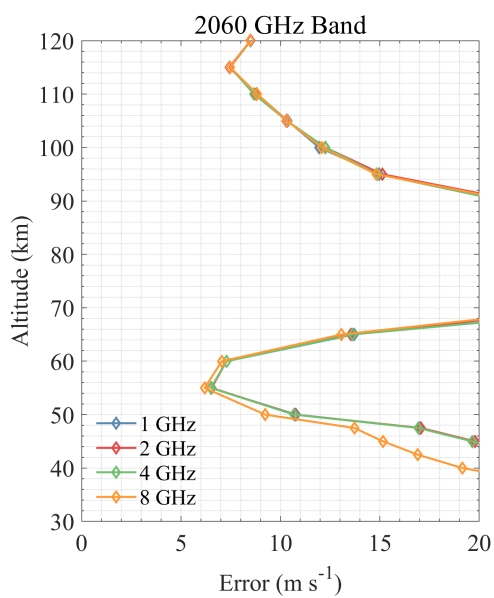**Figure 17.** Same as Fig. 16 but for the 448 and 556 GHz band.
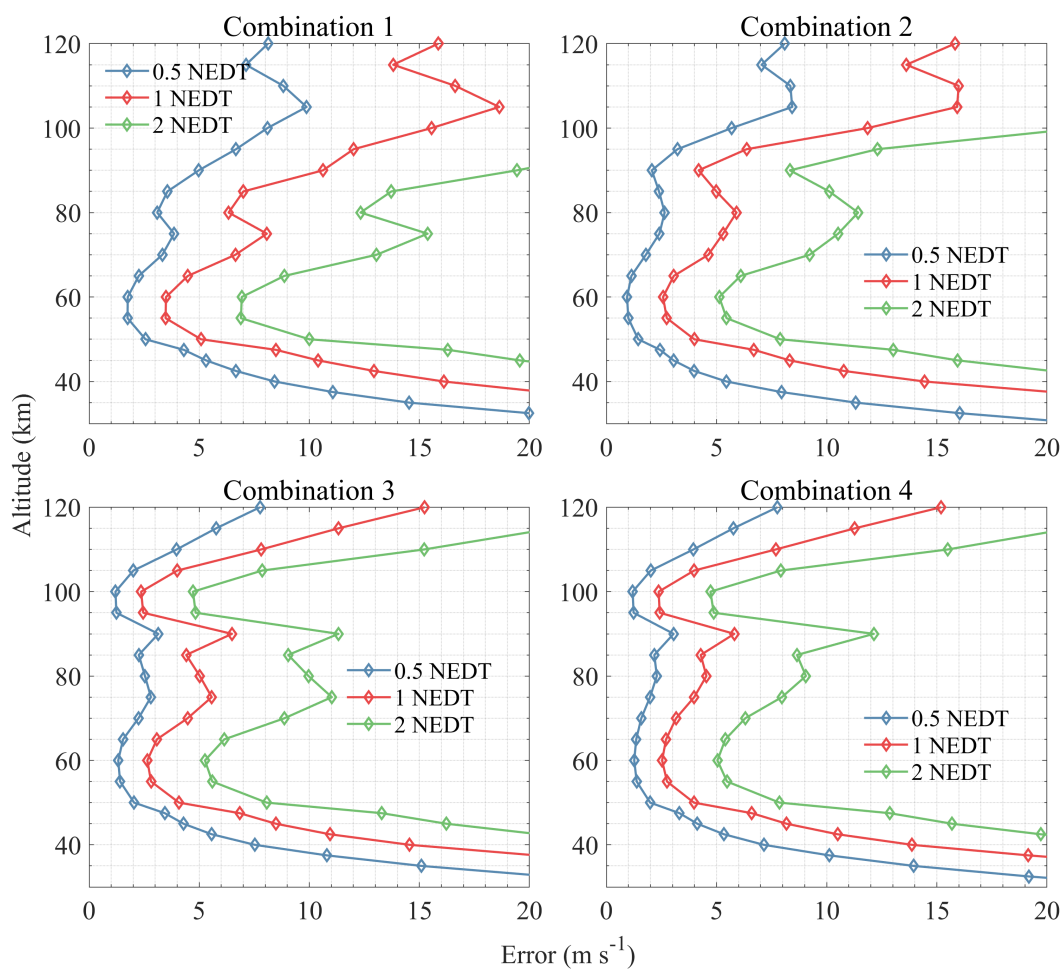


**Figure 18.** Same as Fig. 16 but for the 655 and 840 GHz band.

**Figure 19.** Same as Fig. 16 but for the 2060 GHz band.

**Figure 20.** Performance comparison of different NEDT of the four band combinations.